A Novel Folic Acid-Conjugated TiO_2-SiO_2 Photosensitizer for Cancer Targeting in Photodynamic Therapy

Xiaohui Feng[1‡], Shaokun Zhang[2‡], Hong Wu[2], Xia Lou[1*]

[1.] Department of Chemical Engineering, Curtin University, Kent Street, Bentley, WA 6102, Australia

[2.] Department of Orthopedics, The First Hospital of Jilin University, China

[*] Corresponding author. Department of Chemical Engineering, Curtin University, Kent Street, Bentley, WA 6102, Australia. Tel.: +61 9266 1682; Fax: +61 9266 2681; Email address: X.Lou@curtin.edu.au (X. Lou).

[‡] Equally contributing first authors.

Highlights

- A novel folic acid-conjugated TiO_2-SiO_2 nano-photosensitizer was synthesized for targeted photo-killing of cancer cells

- High photodynamic reactivity, improved cell internalization and cellular and blood compatibility were well demonstrated

- A strong photo-killing effect on the human nasopharyngeal epidermoid cancer (KB) cells was achieved

Graphical Abstract

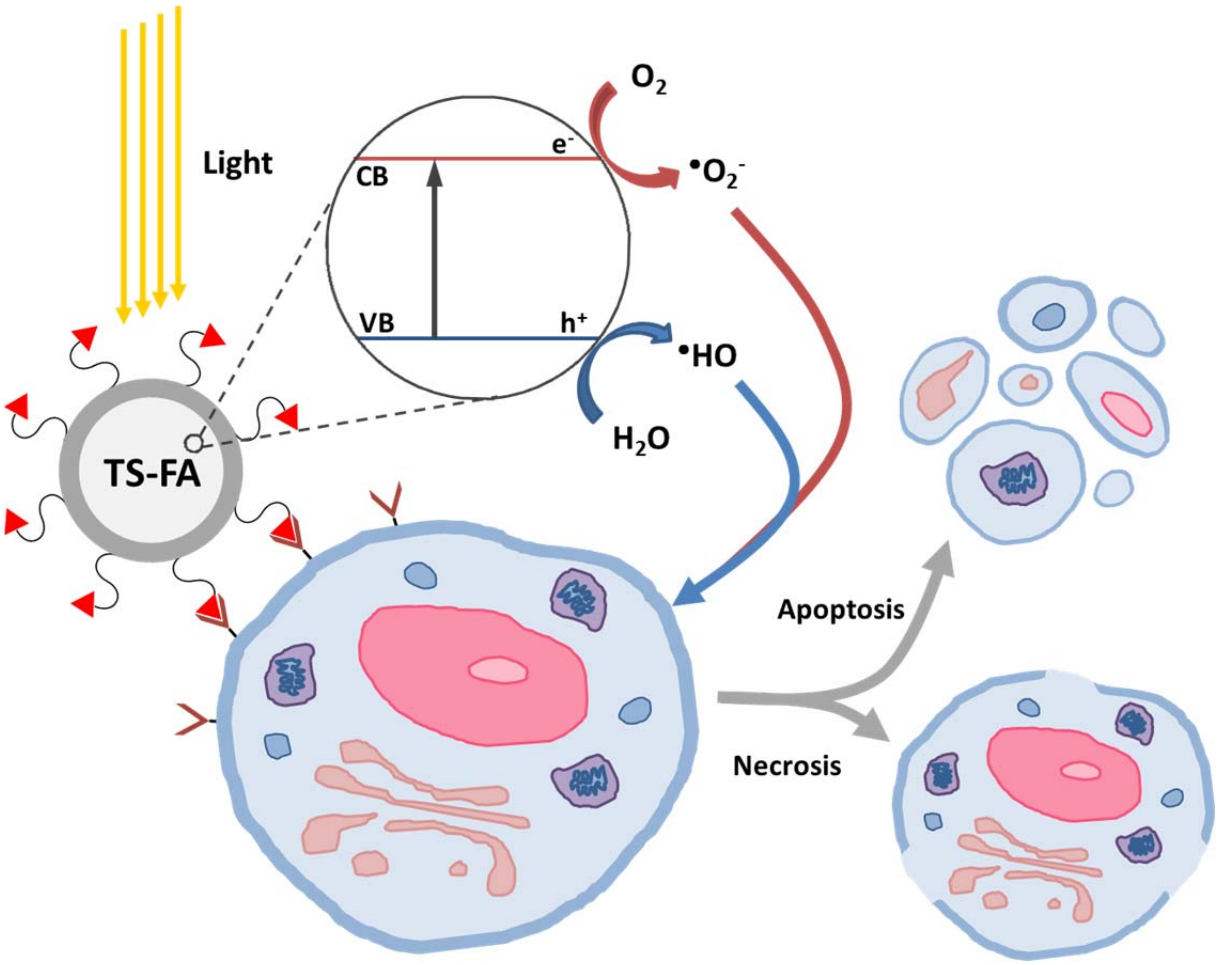

Abstract

In this paper, a novel folic acid-conjugated silica-coated titanium dioxide (TiO_2-SiO_2) photosensitizer was synthesized and characterized using various analytical instruments. The photosensitizer was further assessed in regards to its photoreactivity, cellular and hemocompatibility, cell internalization, and phototoxicity. Conjugating folic acid with TiO_2-SiO_2 has shown a significantly improved compatibility of the nanoparticles with the mouse fibroblast cells (L929) at 24 h. An improved compatibility with the human nasopharyngeal epidermoid cancer (KB) cells was also demonstrated, but to a slightly reduced degree. Enhanced cell internalization was well demonstrated in the TiO_2-SiO_2 folate nanoparticles. Upon exposure to UV light, TiO_2-SiO_2 folate nanoparticles maintained a high level photodynamic reactivity and yielded a 38-43% photo-killing of KB cells. The photo-killing effect increased with increasing dosage in the investigated concentration range of 50-100 μg ml^{-1}.

Key Words: titanium dioxide nanoparticles; targeting; folic acid; photosensitizer, photo-killing; photodynamic therapy.

1. Introduction

Photodynamic therapy (PDT) has been used for the treatment of various cancers and other diseases [1]. It involves the administration of a photosensitizer (PS), either by systemic or topical application, and subsequent initiation of its exposure to light to produce reactive oxygen species (ROS) that kill the cancer cells via the mechanism of apoptosis or necrosis [2]. In addition to directly killing tumor cells, ROS also could damage the blood vessels that supply the oxygen and nutrients to the tumor, leading to tumor shrinkage [3]. Compared to conventional cancer therapy, the major advantages of PDT are that the PS is of low toxicity to normal tissue or cells in the dark, and activation by light alone permits minimal damage to these cells [4]. The combined effect of light and PS makes PDT a selective therapy to use against cancerous or diseased tissue. PDT becomes dual-selective when the accumulation of PS is only on cancer cells, which can be achieved through cell-specific targeting [5].

The commonly used PS drugs are classified as porphyrin-based and nonporphyrin-based. These PSs often contain large π-conjugation domains and are hydrophobic. Their hydrophobic nature causes aggregation of these relatively large molecules under aqueous physiological conditions, resulting in severely reduced ROS formation that is essential for the PDT effect [6, 7]. The poor selectivity to the targeted tissue due to limited accumulation by classic PS drugs also prevents their clinic applications. Skin hyperphotosensitivity and associated pain are ongoing problems for patients after treatment, due to the limited tumor selectivity and slow body clearance of the currently approved PSs [8, 9]. Despite a large number of studies undertaken over the last decades, the limited selectivity and efficacy are still widely accepted problems for PSs associated with PDT treatments. An ideal PS should have the combined properties of high ROS yield and a great degree of selectivity towards the cancerous cells when used in therapeutic concentration, without damaging the healthy tissue.

Titanium dioxide (TiO_2) is a semiconductor-based material, known for its high photosensitivity. It presents a band-gap energy of 3.0 eV. Upon the absorption of a photon with energy that is equal to or higher than this value, TiO_2 can be excited to produce negative electrons in the conduction band, leaving positive holes in the valence band. These charge carriers react with surrounding water or oxygen to yield cytotoxic ROS such as hydroxyl (•OH), hydrogen peroxide (H_2O_2), and superoxide ($\bullet O_2^-$). Both the generated holes and ROS are strong oxidizers that can attack cell membranes and other cellular components, leading to apoptosis of cancer cells [10]. TiO_2 nanoparticles also have been proven to be effective in

preventing drug efflux caused by multi-drug resistance (MDR), leading to selective accumulation of TiO_2 at the tumor site [11, 12]. They have shown good cytocompatibility in the dark, both *in vitro* and *in vivo* [13]. Clinical application of TiO_2 is limited, mostly due to the aggregation of the nanoparticles that leads to a decrease in photocatalytic reactivity [14], and the lack of specificity to target the cancerous cells. We have demonstrated that encapsulating TiO_2 within a silica shell can improve both the dispersion and cell compatibility of the nanoparticles, whilst maintaining high photodynamic reactivity [10]. The aim of this study is to synthesize folic acid-conjugated (FA-conjugated) TiO_2, via the functionalized silica shell, and to investigate the cell internalization and cytotoxicity of these nanoparticles, both in the dark and under irradiation, so as to develop a high performance and targeted photosensitizer for cancer treatments that utilize PDT.

FA-conjugated silica-coated TiO_2 (TS-FA) nanoparticles were prepared according to the reaction scheme illustrated in Fig. 1. First, silica-coated TiO_2 (TS) was synthesized according to our previous work, which was further aminated using (3-aminopropyl)triethoxysilane (APTES) to produce amine-terminated silica-coated TiO_2 (TS-NH_2) nanoparticles. N-Hydroxysuccinimide-ester of folic acid (NHS-FA) then was prepared using the N, N'-Dicyclohexylcarbodiimide (DCC)-based coupling reaction, and further reacted with TS-NH_2 to produce FA-conjugated TiO_2 (TS-FA) nanoparticles. The chemical and surface properties of the produced compounds were characterized using Fourier transform infrared (FTIR) spectroscopy and thermogravimetric/differential thermal analysis (TG/DTA). The size and morphology of the obtained nanoparticles were examined using a field emission scanning electron microscope (FESEM) and a high-resolution transmission electron microscope (HRTEM). The photocatalytic properties of TS, TS-NH_2 and TS-FA nanoparticles were examined on the basis of photodecomposition of phenol, an organic pollutant that has been used as a model chemical to evaluate photocatalytic activity of various photocatalysts. The cytotoxicity, hemocompatibility, and phototoxicity of selected nanoparticles were assessed using both the primary adherent mouse fibroblast connective tissue cells (L929), and human nasopharyngeal epidermoid cancer (KB) cells. The cell internalization of TS-FA nanoparticles was evaluated using KB cells as the positive folate receptor cells. Findings show that the TS-FA nanoparticles can be used as an effective photosensitizing agent for active targeting of cancer cells.

2. Materials and methods

2.1 Materials

Degussa P25 was purchased from Degussa. Tetraethyl orthosilicate (TEOS, 99.999%), (3-aminopropyl)triethoxysilane (APTES, ≥99%), absolute ethanol (≥99.5%), N-Hydroxysuccinimide (NHS, 98%), N, N'-Dicyclohexylcarbodiimide (DCC, 99%), triethylamine (≥99%), folic acid (FA, ≥97%), sodium carbonate ($NaCO_3$, ≥99.5%), and sodium bicarbonate ($NaHCO_3$, 99%) were purchased from Sigma-Aldrich. Diethyl ether anhydrous (≥99.0%) and dimethyl sulfoxide (DMSO, 99.9%) were purchased from Alfa Aesar. Milli-Q water was used in all experiments.

2.2 Chemical synthesis

TS-NH_2 nanoparticles were first prepared using the sol-gel method (Fig. 1). In brief, TiO_2 nanoparticles (0.1 g, 1.3 mmol) were suspended in a solution containing 20 ml of ethanol, 60 ml of Milli-Q water and 1 ml of ammonia solution, using ultrasonic vibration for approximately 30 min. Then, 20 ml of ethanol containing TEOS (40 μl, 0.18 mmol) was added, dropwise, to the mixture under magnetic stirring. The reaction was maintained at room temperature for 2 h. TS-NH_2 nanoparticles were subsequently obtained by the addition of 20 ml ethanol solution containing APTES (81 μl, 0.36 mmol), resulting in the molar ratio of APTES to TEOS being 2:1. The reaction mixture was then heated up to 90 ^oC and kept at this temperature for a further 2 h. Following this, the reaction mixture was allowed to cool down to room temperature and centrifuged at 7500 rpm for 10 min. The liquid was discarded and the TS-NH_2 nanoparticles were washed three times with 15 ml of ethanol (3×15 ml), followed by three times with 15 ml of Milli-Q water (3×15 ml) and dried overnight at room temperature under vacuum.

NHS Folate (NHS-FA) was obtained through the DCC coupling reaction (Fig. 1). In brief, folic acid (5.0 g, 11.3 mmol) and triethylamine (1.8 g, 17.9 mmol) were added to 100 ml of freshly distilled dimethyl sulfoxide (DMSO) at room temperature under constant stirring. After stirring for 2 h, NHS (2.6 g, 22.6 mmol) and DCC (4.7 g, 22.8 mmol) were added to the mixture. The obtained reaction mixture had a molar ratio of 1.0 folic acid: 1.6 triethylamine: 2.0 NHS: 2.0 DCC. The reaction was allowed to proceed overnight in the dark. Then, the dicyclohexylurea by-product was removed by filtration and the liquid was concentrated in the

presence of reduced pressure and heating. The concentrated liquid (1.5 ml) was dispersed in THF (15 ml) with constant shaking to remove the excess amount of DMSO. Then, anhydrous diethyl ether (5 ml) was added into the mixture and the characteristic yellow powder was formed, followed by collection via centrifugation at 7500 rpm for 10 min. The liquid was discarded. After that, the solid was dispersed into 15 ml of a mixture of THF/anhydrous diethyl ether (3:1), and the whole procedure was repeated five times. The resultant NHS-FA was dried under vacuum, overnight, to remove any residual ether and THF, and then stored at 4 ^{o}C in the dark.

TS-FA nanoparticles were finally produced through a reaction of the NHS groups of the above obtained NHS-FA with the primary amine presented on the surface of TS-NH_2 (Fig. 1). TS-NH_2 nanoparticles (100 mg) were suspended in 10 ml of sodium carbonate/bicarbonate buffer solution (0.01 M, pH=9.0) using ultrasonic vibration at room temperature. Then, NHS-FA (289 mg) was dissolved into dry DMSO (10 ml) under magnetic stirring. The solution of NHS-FA in DMSO was added, dropwise, to the obtained nanoparticle suspension and the reaction was maintained at room temperature with constant stirring. After stirring in the dark for 2 h, the derived TS-FA nanoparticles were collected using a centrifuge at 7500 rpm for 15 min. The product was washed with DMSO (3×15 ml), followed by ethanol (1×15 ml), and dried overnight under vacuum.

2.3 Characterization of TS-NH_2, NHS-FA, and TS-FA

Scanning electron micrographs of all nanoparticles produced were obtained using a FESEM (Zeiss Neon 40EsB FIB-SEM). Prior to FESEM examination, the sample suspension in Milli-Q water (20 μg ml^{-1}) was mounted on an aluminum stub. The aluminum stub was allowed to air-dry at ambient temperature overnight and then coated with platinum (2 nm) which was used as a conducting surface material. Operation of the microscope was carried out at an accelerating voltage of 5 kV. The mean diameter of the particles was analyzed using the SmartSEM software that was related to the scale bar for the recorded FESEM images. Sixty particles were randomly selected for size measurements.

The detailed morphology of the produced nanoparticles also were visualized using HRTEM (JEOL 3000F). The sample preparation for HRTEM examination was performed by placing one drop of the sample dispersion in ethanol solution (10 μg ml^{-1}) on a copper grid with a substrate of carbon film and air-dried at room temperature overnight. HRTEM images

of the nanoparticles were recorded at an accelerating voltage of 200 kV. The sizes of the nanoparticles were measured using the in-built JEOL operational software, DigitalMicrograph, which also was linked to the magnification scale bar of the obtained TEM images.

The surface chemistry of the produced TS, TS-NH_2 and TS-FA nanoparticles were characterized using a Thermo Scientific Nicolet iS50 FTIR spectrometer fitted with a diamond ATR sampling accessory. An FTIR spectrum of each sample was recorded between 200 and 4000 cm^{-1}.

The relative amounts of the organic compounds presented on the surface of the samples were determined through burning the elements of carbon, nitrogen and hydrogen in air with a flow rate of 0.1 L min^{-1}, and then calculated using the data obtained from TGA-DSC (Mettler-Toledo Star^e). The obtained nanoparticles (10-15 mg) were heated from 35 ^oC to 900 ^oC in air with a heating rate of 10 ^oC min^{-1}.

Nuclear magnetic resonance (NMR) spectroscopy was conducted on a Bruker Advance III NMR spectrometer (400 MHz), using dimethyl sulfoxide (DMSO)-d_6 as the solvent. To prepare the sample for ^1H NMR examination, NHS-FA (10 mg) was dissolved in DMSO-d_6 (1 ml) and the mixture was added into the dry NMR tube.

The amine groups on the surface of TS-NH_2 particles were quantified using a back titration method [15]. In brief, TS-NH_2 nanoparticles (10 mg) and HCl aqueous solution (40 ml, 1.0 mM) were mixed with constant stirring for 2 h. Then, the mixture was separated using a centrifuge and the solid was discarded. The liquid was collected and titrated using an aqueous solution of NaOH (1.0 mM). Two drops of phenolphthalein in ethanol solution were added as a pH indicator.

2.4 Photoreactivity study

The photoreactivity of TS-NH_2 and TS-FA nanoparticles was determined based on phenol degradation efficiency. Pure TiO_2 (P25) and the silica-coated TiO_2 (TS) containing no folic acid also were assessed for comparison purposes. In brief, a preferred amount of catalyst was mixed with phenol solution (200 ml, 20 μg ml^{-1}) with constant stirring. The reaction was performed in a 1 L double-jacketed reactor that was connected to a water bath through a pump to maintain the reaction temperature at 25±1 ^oC. The light source was provided by an MSR 575/2 metal halide lamp (575 W, Philips) with a wavelength between 315 and 1050 nm. For

the first 30 min, the reaction mixture was stirred in the dark to reach the adsorption-desorption equilibrium. After this, the reaction was carried out under light. At the prescribed time intervals, 5 ml of the catalyst suspension in phenol solution was withdrawn and the solid in the suspension was filtered using a 0.45 μm Millipore filter. The liquid was reserved and sent for analysis using an HPLC (Varian) in which the UV detector was adjusted to 270 nm. The concentration of TiO_2 for phenol degradation was kept at 0.25 g L^{-1} for all nanoparticles.

2.5 Cell culture and nanoparticle preparation

Human nasopharyngeal epidermoid cancer (KB) cells (ATCC, USA) were grown in RPMI-1640 folic acid-deficient medium supplemented with 10% fetal bovine serum and 1% L-glutamate (Gibco® by life Technologies™). Primary adherent mouse fibroblast connective tissue cells (L929), also from ATCC, were maintained in Dulbecco's modified Eagle's medium (DMEM) with 10% FBS. The cells were grown into 96-well plates at a density of 1×10^4 cells per well at 37 ^oC and under 5% CO_2. P25, TS, and TS-FA nanoparticles of varying concentrations were dispersed into the growth medium for different assessments.

2.6 MTS assay

The MTS assay measured the absorbance of the formazan product which is formed by the reduction of [3-(4, 5-dimethylthiazol-2-yl)-5-(3-cayboxymethoxyphenyl)-2-(4-sulfophenyl) -2H-tetrazolium] (MTS) using dehydrogenase enzymes in living cells. The formed formazan product, recorded at 490 nm, is proportional to the number of living cells in the growth medium. A detailed description of the cytotoxicity assessment can be found in our previous paper [10]. For this work, the particle concentrations involved in MTS analysis were 12.5, 25, 50, 100, and 200 μg ml^{-1}, respectively. A control experiment was performed using the cells treated with complete medium involving no particles, under identical conditions. Cells were incubated with the nanoparticles for 6 h and 24 h, respectively, prior to the MTS assessment. The relative cell viability was estimated by $A_{test}/A_{control}$, where A_{test} and $A_{control}$ are the absorbance of the produced formazan by samples and controls, respectively. It should be noted that all the experiments were repeated three times in the dark. The live/dead cells were recorded by an Olympus BX61 microscope.

2.7 Hemolysis assay

Rabbit red blood cells (RBCs) were used for hemolysis studies of the samples using our reported procedure [10]. The sample concentrations were 12.5, 25, 50, 100, and 200 μg ml^{-1}, respectively. For control purposes, the mixture of the RBC suspension (100 μl) and PBS buffer (100 μl) was applied as a negative control, while that of the RBC suspension (100 μl) and 0.5% Triton X-100 (100 μl) was used as a positive control. The percentage hemolysis was estimated using the equation below:

$$\text{Hemolysis}(\%) = \frac{A_{576,\text{ sample}} - A_{576,\text{ negative control}}}{A_{576,\text{ positive control}} - A_{576,\text{ negative control}}} X\,100\% \quad (1)$$

Where $A_{576,\text{ sample}}$, $A_{576,\text{ negative control}}$, and $A_{576,\text{ positive control}}$ represent the absorbance of hemoglobin released from particle-treated RBCs, PBS buffer treated RBCs, and medium involving 0.5% Triton X-100 treated RBCs, respectively.

2.8 Photo-killing effect

To investigate the photo-killing effect of the derived nanoparticles under light, the cultured KB cells were trypsinized and suspended into culture medium at a concentration of 5.0×10^4 cells/ml. Then, each well in a 96-well plate was injected with 200 μl of the seeding cells. The plate was put into an incubator at 37 ^oC under 5% CO_2. After being incubated overnight, the cell medium was replaced with the medium consisting of P25, TS or TS-FA nanoparticles, each at the concentrations of 12.5 and 50 μg ml^{-1}. The cells were incubated for 24 h in the dark and then were illuminated with UV light (365 nm, 50 W). After 10 min illumination, the cells were removed from UV radiation and incubated overnight at 37 ^oC under 5% CO_2. A control experiment was carried out using the cells treated with complete cell medium under the same experimental conditions. The cell viability also was evaluated using an MTS assay. The surviving fraction of KB cells is expressed as the ratio of the absorbance level of cells exposed to UV light to that of cells in the dark. All the experiments were performed in triplet.

2.9 Cell internalization

Prior to the cell internalization experiment, P25, TS, and TS-FA particles (20 mg each) were separately suspended in a 0.5 ml acetone solution of fluorescein isothiocyanate (FITC)

(1.0 mg ml^{-1}). The suspensions were shaken overnight. Then, the particles were collected, using a centrifuge at 7500 rpm, and washed multiple times with Milli-Q water until the supernatant was clear. The resultant FTIC-labeled nanoparticles were then re-suspended into culture medium for further investigation.

To determine the intracellular uptake of the derived particles, KB cells, at a density of 1×10^5 cells per well, were plated in a 12-well polystyrene dish and incubated at 37 ^oC and under 5% CO_2. After incubation overnight, the culture medium was substituted with fresh medium containing the labeled nanoparticles, each at the concentration of 100 μg ml^{-1}. Then cells were returned to the incubator under 5% CO_2. After 6 h of incubation, the medium was removed from each sample and the cells were washed in triplet with PBS (pH 7.4) to clear the unattached particles away. Then the cells were fixed with 4% formaldehyde in PBS for 15 min and, subsequently, the fixed cells were visualized using a confocal laser scanning microscope with an FITC filter.

2.10 Statistical analysis

The results were expressed as mean±standard error. All the data were statically analyzed using Student's T-test. Statistical significances were considered at $p<0.05$.

3. Results and Discussion

3.1 Characterization of NHS-FA

FTIR was used to characterize NHS-FA in comparison with pure FA, as displayed in Fig. 2a. For FA, the peaks in the 2900-3600 cm^{-1} region are assigned to the -OH stretching vibrations of L-glutamic acid moiety and the –NH···H stretching vibrations of the pterin ring [16]. The peak at 1694 cm^{-1} belongs to the C=O stretching vibration of the –COOH group while the peak at 1640 cm^{-1} relates to the C=O stretching vibration of the –CO-NH- (amide band II) group from the L-glutamic acid moiety [17]. Also, the –NH stretching vibration of the –CO-NH (amide band II) group appears at 1570 cm^{-1} [18]. The absorption peaks at 1485 and 1414 cm^{-1} are attributed to the phenyl ring and the –OH deformation band of the phenyl skeleton, respectively. After NHS was used to activate FA, the successful formation of NHS-FA was confirmed via two notable absorption peaks at 1201 and 1068 cm^{-1}, corresponding to the C-O and N-O stretching vibrations, respectively, of the newly formed succinimidyl ester group [19]. Additionally, there is a strong peak at 1729 cm^{-1} that is due to

splitting of the band associated with the C=O stretching vibration of the newly formed succinimidyl ester group. The absorption peaks at 1814 and 1782 cm^{-1} are related to the C=O stretching vibration of the succinimidyl carbonyl groups [20]. Other absorption peaks below 1400 cm^{-1} correspond to various vibration modes related to the ring structure of the pterin moiety [17].

^{1}H NMR was used to further confirm the successful synthesis of NHS-FA. In the ^{1}H NMR spectrum of NHS-FA (Fig. 2b), the signals at 2.50 and 3.30 ppm belong to the DMSO-d_6 and water, respectively. The signal at 11.35 ppm is attributed to the –OH proton in the carboxylic group of FA, while the signals at 8.65, 7.64, and 6.65 ppm are due to the aromatic protons of FA [21]. The signals presenting at 7.00 and 8.13 ppm belong to the –NH- protons in the p-amino benzoic acid moiety and the –CO-NH- in the glutamate moiety of FA, respectively [22]. The methylene protons in the pterin moiety and the glutamate moiety of FA appear at 4.48, 2.31, and 1.99-2.10 ppm, while the methylene protons of NHS can be observed at 2.8 ppm, indicating that FA has been successfully converted to NHS-ester of folic acid via DCC as a coupling agent [23]. The integration at 2.8 ppm revealed a higher than stoichiometric value (5.19 against 4), which is probably due to the presence of unreacted NHS.

3.2 Characterization of TS-NH_2 and TS-FA nanoparticles

FESEM images, presented in Fig. 3a, indicate that the morphology of the P25, TS, TS-NH_2, and TS-FA were generally the same. The sizes of TS, TS-NH_2, and TS-FA were 35±2 nm, 39±5 nm, and 43±3 nm, respectively, indicating a gradual increase of particle size in comparison with P25 (24±1 nm). The TEM images in Fig. 3b reveal a clear core-shell structure of TS, TS-NH_2, and TS-FA nanoparticles. The size increases of these particles also are evident in comparison with the non-coated TiO_2. For TS-NH_2, the core nanoparticles with well-defined crystal facets were evident via the obvious lattice fringes, which, at 0.35 nm, correspond to the d-spacing for (101) lattice planes of anatase TiO_2 nanoparticles. The coated silica layer is amorphous and the relative thickness is approximately 3 nm. After further conjugation with FA, the outer layer of TS-FA nanoparticles increased up to approximately 5 nm. The lattice fringes of the core nanoparticles are at 0.32 nm and 0.35 nm, which agrees well with d-spacings of the (110) plane in rutile TiO_2 nanoparticles and the (101) plane in anatase TiO_2 nanoparticles, respectively.

The FTIR spectra of all samples in the region of 100-4000 cm^{-1} are shown in Fig. 4a. The FTIR peaks located at 630 and 388 cm^{-1} are attributed to the stretching vibration of Ti-O groups, confirming the presence of TiO_2 in all samples. After a silica layer was applied to the TiO_2 nanoparticles, the successful formation of the silica network was proven via the characteristic absorption peaks at 1065 cm^{-1} and 1156 cm^{-1}, representing the bending and stretching vibrations of the Si-O-Si groups. Additionally, a weak peak at 950 cm^{-1} is attributable to the formation of Ti-O-Si linkage between TiO_2 core nanoparticles and the silica layer, via condensation. The broad peak at 3350 cm^{-1}, presented in all samples' spectra, is assigned to the stretching vibration of O-H groups from the adsorbed water [10], and the absorption peak at around 2150 cm^{-1} is from CO_2 in air.

The expanded spectra of TS-NH_2 and TS-FA in the region 1300-1700 cm^{-1} are shown in Fig. 4b. The two characteristic peaks of TS-NH_2, at 1560 and 1491 cm^{-1}, correspond to the bending vibration of –NH_2 [24]. The weak absorption peaks located at 1413, 1444, and 1472 cm^{-1} are attributed to the bending vibration of –CH_2 groups in the n-propyl chain from APTES moieties [25]. After binding FA with the primary amine groups, the characteristic peak at 1560 cm^{-1} disappeared and a new absorption peak at 1606 cm^{-1}, corresponding to the –NH stretching vibration from the –CO-NH- (Amide II) groups, was observed [26]. Meanwhile, the characteristic peak at 1628 cm^{-1} is associated with the C=O stretching vibration of the –CO-NH- (Amide I) groups. Those observations indicated that FA was covalently linked to the surface of TS-NH_2 through the amide bond. The peaks at 1400 cm^{-1}, 1450 cm^{-1}, and 1512 cm^{-1} further demonstrated the presence of–COO and C=C groups in TS-FA.

To verify the content of the –NH_2 groups and FA groups in TS-NH_2 and TS-FA nanoparticles, the TGA analysis was carried out in the presence of air. As shown in Fig. 5a, a two-stage mass loss was observed in both compounds. When the temperature was in the region of 35-110 ^oC, a slight mass loss was observed due to the release of absorbed water molecules. There was a significant decrease in mass when the temperature was between 110 and 850 ^oC. This can be assigned to the release of CO_2, CO, NO_2, or H_2O owing to the decomposition of organic groups grafted onto the surfaces of the particles [27, 28]. The weight losses for P25, TS, TS-NH_2, and TS-FA nanoparticles in the region of 110-850 ^oC were 0.7, 1.8, 3.2, and 8.0 wt%, respectively. Assuming that all the ethoxy groups were removed after the condensation of TEOS, then the mass loss of TS-NH_2 must have been from the $CH_2CH_2CH_2NH_2$ of APTES. Hence, the surface density of –NH_2 was calculated to be

0.23 mmol g^{-1}. The back titration method yielded an average surface density of amine groups of 0.20 mmol g^{-1}, which is comparable to the data obtained from TGA.

3.3 Photocatalytic reactivity

The photoreactivity of the obtained nanoparticles was evaluated on the basis of phenol degradation in the presence of UV light. Fig. 5b shows the percentage degradation of phenol using P25, TS, TS-NH_2, and TS-FA at the given time intervals. Upon exposure to UV light for 150 min, complete removal of phenol with an initial concentration of 20 μg ml^{-1} was obtained. In the presence of TS, TS-NH_2, and TS-FA, the values of percentage degradation of phenol were 70%, 10%, and 67%, respectively. The apparent rate constants of these nanoparticles were valued using the Langmuir-Hinshelwood equation, where k represents the apparent reaction rate constant in the unit of min^{-1}, and C_0 and C are the phenol concentrations at t=0 and t=t, respectively:

$$\ln \frac{C}{C_0} = -\kappa t \qquad (2)$$

The computed k values for P25, TS, TS-NH_2, and TS-FA were 0.0242, 0.0084, 0.0005, and 0.0066 min^{-1}, respectively. The irradiation time used was 120 min. The corresponding least squared R values for each sample were 0.973, 0.989, 0.957, and 0.969, respectively.

The reduction of photodegradation rate after the encapsulation of TiO_2 in silica shell is consistent with our previous observation, which is mostly due to the shielding effect of the silica matrix and the increase in nanoparticle sizes [10]. Folation of the TS nanoparticles has resulted in a slight reduction of the degradation rate constant from the 0.0084 min^{-1} of TS to 0.0066 min^{-1} of TS-FA, which is probably due to the increased size of TS-FA. A very low value of rate constant was shown by the intermediate TS-NH_2 nanoparticles, which is probably due to the competing photo-oxidation of primary amine groups on the surface of the TS-NH_2. A study has shown that, under UV illumination, the ROS generated from photoexcited TiO_2 nanoparticles can oxidize primary amine groups to yield NO_3^- ions, and the cleavage rate of the C-N bond from primary amine is faster than that of the C-C bond in the hydrocarbon molecules [29].

3.4 Cytotoxicity and hemocompatibility study

3.4.1 Toxicity of P25, TS, and TS-FA to L929 and KB cells

Fig. 6a displays the relative viability of L929 cells after 6 h and 24 h incubation with P25, TS, and TS-FA of various concentrations (0, 12.5, 25, 50, 100, and 200 μg ml^{-1}). The culture was performed in the dark. When the incubation time was 6 h, there were no significant differences between the untreated cells and cells treated with P25, TS, TS-NH_2, and TS-FA nanoparticles. The viability of L929 cells, in relation to the control, was well above 90% for all. Upon prolonged incubation time to 24 h, a dramatic increase in cell viability was observed in the presence of TS-FA over the investigated concentration range. A decrease of cell viability to 82% was observed when P25 (200 μg ml^{-1}) was added to the cells. No significant change was observed in the viability of the cells treated with TS nanoparticles. It is known that the silica coating reduces the cytotoxicity of core nanoparticles [10]. For TS-FA-treated cells, the viability was about two-fold greater than that of both untreated cells and cells treated with other nanoparticles. The enhanced cell proliferation may be because folic acid, an essential vitamin B element for cell proliferation, promoted the cell growth.

A toxicity study of P25, TS, and TS-FA nanoparticles on KB cells also was conducted. The study was carried out by exposing the cells to the nanoparticles at the prescribed concentrations, shown in Fig. 6b. Similar to the results for the L929 cells, after 6 h incubation, no apparent differences in cell viability ($^{*}p>0.05$) were observed between control cells and cells treated with P25, TS, and TS-FA over the investigated concentrations. When the incubation time was increased to 24 h, the viability of TS-treated cells was decreased to 73.3% and 79.7%, respectively, in the presence of 100 and 200 μg ml^{-1} of nanoparticles. The toxic effect of TS nanoparticles on KB cells in the dark is possibly due to the higher toxicity of silica towards cancerous cells [30]. This is indeed true when comparing the KB cell viability with the L929 cell viability after the cells were treated with TS nanoparticles. In the presence of 100 and 200 μg ml^{-1} of TS nanoparticles, the cell viability was 98.5% and 96.5% respectively for L929, and 73.3% and 79.7% for KB cells (Fig. 6). We speculate that the viability of TS-treated cells vary from one cell line to another. Similar results have been reported by other researchers [31].

For TS-FA-treated KB cells, a concentration-dependent increase in viability was observed, which further demonstrates the nutritional effect of the folate component in the nanoparticles.

It is interesting to note that TS-FA also displayed a degree of toxicity towards the cancerous KB cells. This is particularly obvious at the lower concentration range. For instance, when the concentration of TS-FA was 12.5, 25, and 50 μg ml^{-1}, the cell viability for L929 was 200%, 196%, and 196%, respectively, whilst that for KB cells was 173%, 182%, and 194%. The overall enhancement in cell proliferation by TS-FA nanoparticles was demonstrated for both L929 and KB cells. Repeated experiments show similar effect. This could be a result of high FA-composition in the TS-FA nanoparticles. As we know that folic acid is often used in the growth medium to promote cell growth. In a standard growth medium, the concentration of folic acid is approximately 1.01 μg ml^{-1} [32]. In this study, the produced TS-FA contained 4.8% of FA, according to the TGA analysis. This would lead to a FA concentration of 0.6, 1.2, 2.4, 4.8, and 9.6 μg ml^{-1}, respectively, when 12.5, 25, 50, 100, and 200 μg ml^{-1} TS-FA was added to the culture medium. Most of these concentrations are higher than that of folic acid in the standard growth medium. The promotion of KB-cell growth by folate conjugated quantum dots was also reported by other researchers [33]. They found that after 24 h of incubation, the viability of KB cells that have been treated with FA-conjugated QD nanoparticles was 1.2 times greater than that of untreated cells at the particle concentration of 200 nmol L^{-1}. The impact of FA-component on the cell viability at an earlier time, i.e., 6 h, was not as significant as that at 24 h. This could be due to the limited interaction time between cells and the nanoparticles.

3.4.2 Hemocompatibility study

Fig. 7a shows the *in vitro* hemolysis results of P25, TS, and TS-FA at a similar particle concentration range. The detected hemoglobin release is well below 5% over the investigated concentration range, indicating a good compatibility of these nanoparticles with the blood cells. A relatively high hemolysis activity was seen when the RBC was treated with the nanoparticles at a particle concentration of 50 μg ml^{-1}. The activity was reduced at both a higher and a lower concentration. We speculate that, although increased amounts of nanoparticles lead to more active hemolysis, it also increases the opportunity for the nanoparticles to aggregate, thereby decreasing the surface area that can interact with the RBCs.

3.5 Photo-killing effect

Based on the above observations, the photo-killing experiments were carried out on KB cells in the presence of P25, TS, and TS-FA nanoparticles after the cells had been incubated with the nanoparticles for 24 h. The influence of UV irradiation alone on KB cells was first assessed. The observed relative surviving fractions of the KB cells were 100%, 96%, 99%, and 90% at 10 min, 20 min, 45 min, and 60 min, respectively. The exposure time of 10 min was chosen for the photo-killing investigations of the selected nanoparticles and the results are shown in Fig. 7b. The surviving fraction of cells was reduced from 100% for the control to 93%, 78%, and 82% in the presence of 12.5 μg ml^{-1} of P25, TS, and TS-FA, respectively. The reductions for both TS and TS-FA were both similar and significant in comparison with the control cells ($^{*}p<0.05$). As the concentration of the nanoparticles was increased to 50 μg ml^{-1}, the surviving fractions became 80%, 73%, and 62% for KB cells treated by P25, TS, and TS-FA, respectively. At this concentration, the killing effect was apparent for all nanoparticles investigated. In comparison with P25-treated cells, a statistically significant ($^{**}p<0.05$) photo-killing effect of TS-FA on KB cells was evident. The viability of KB cells was further reduced to 57% when the TS-FA concentration was increased to 100 μg ml^{-1}. Cell internalization of TS-FA was well demonstrated in the fluorescence confocal micrographs (Fig. 8a). In comparison with TS-FA, the fluorescence in P25 treated cells is relatively weak. There is no fluorescence seen in both the control cells and the TS-treated cells. The phase contrast images (Fig.8b) further demonstrated that the dosage of P25 internalized by KB cells is generally lower than that of TS-FA. This is most likely due to the presence of the folate component on the surface of TS-FA nanoparticles, which are able to be specifically bound with the folate receptors on the folate-receptor positive KB cells. It is apparent that the higher photo-killing effect of the TS-FA nanoparticles also is associated with the stronger cell internalization. It should be noted that 194% of viable KB cells were observed when they were treated with the same amounts of TS-FA in the dark for 24 h. The detected photo-killing effect of TS-FA in the previous section could have been reduced by such enhanced growth. A higher photo-killing power can be achieved by fine tuning the nanoparticles by controlling the FA density on the surface of the nanoparticles. To the best of our knowledge, this is the first study on folic acid-conjugated titanium dioxide-silica (TS-FA) nano-photosensitizer for effective PDT. Early studies on pure TiO_2 nanoparticles by Cai et al. have shown a complete photo-killing of HeLa cells after 10 min exposure to a Hg-lamp (500 W) [13]. There was no indication of the effect to the cells by the high power radiation alone. Antibody has been used

for cell specific targeting using TiO_2 nanoparticles for effective PDT. One study [34] has shown that, with 30 min irradiation of a UV-light at 365 nm, the surviving fraction of LoVo cells was reduced from 84% to 67% due to the presence of 3.12 μg/ml antibody-modified TiO_2 nanoparticles. No data was reported about the effect of higher concentration nanoparticles. A similar study was reported by a different group, in which 80% cell death (by cell counting) was induced by the polyacrylic acid-coated TiO_2 that is modified with anti-epidermal growth factor receptor antibody [35]. No control data was provided in this study. Nitrogen-doped TiO_2 nanoparticles was also investigated for visible light irradiation induced PDT, however no targeting ligand was considered [36].

4. Conclusions

In summary, a novel folic acid-conjugated titanium dioxide-silica core-shell nanoparticulate system, TS-FA, was fabricated using the commercially available semiconductor photocatalyst, P25, and confirmed by various chemical and physical characterization methods. Investigations on the cytotoxicity and hemocompatibility showed that the produced TS-FA nanoparticles are nontoxic to both L929 and KB cells in the dark, and are well tolerated by human red blood cells. A strong increase in viability of both L929 and KB cells was demonstrated after cells were incubated with TS-FA in the range between 12.5 and 200 μg ml^{-1}, showing that the presence of the folate element acts as a nutrient for the cells. Upon exposure to UV light for 10 min, both P25 and TS-FA were toxic to KB cells due to their high photocatalytic activities. The cell internalization experiments proved that folic acid-conjugated nanoparticles were bound to the folate receptor-positive KB cells, indicating a high ability to target cancerous cells. The dual targeting capabilities, through both the folic acid conjugation and high photoexcitation efficiency of the TS-FA system, promises great potential in the treatment of cancer, and possibly other diseases. It is worth noting the strong concentration dependence of the photo-killing effects that was observed in the cells exposed to TS-FA, and the improved compatibility of TS-FA with both L929 and KB cells due to the 'nutritional effect' of the folate components in the nanoparticles. Although a high photo-killing effect of 38-43% on the KB cells has been achieved in this study, the nanoparticulate system can be further tuned to maximize its photo-killing power. A systematic study is under way to optimize the folate content in the nanoparticles so as to achieve an optimal photo-killing ability to a greater variety of cancerous cells. The development and

application of high performance nano-photosensitizers for the use in PDT is a topic of on-going study [5, 10, 37].

References

[1] B.C. Bae and K. Na, Biomaterials 31 (2010) 6325.

[2] D.E.J.G.J. Dolmans, D. Fukumura and R.K. Jain, Nat. Rev. Cancer 3 (2003) 380.

[3] B.W. Henderson and T.J. Dougherty, Photochem. Photobiol. 55 (1992) 145.

[4] L.M. Davids and B. Kleemann, Cancer Treatment Rev. 37 (2011) 465.

[5] A. Master, M. Livingston and A.S. Gupta, J. Controlled Release 168 (2013) 88.

[6] R.W. Boyle and D. Dophin, Photochem. Photobiol. 64 (2008) 469.

[7] F. Ricchelli, J. Photochem. Photobiol. B 29 (1995) 109.

[8] E. Paszko, C. Ehrhardt, M.O. Senge, D.P. Kelleher and J.V. Reynolds, Photodiagnosis Photodyn Ther 8 (2011) 14.

[9] I.J. Macdonald and T.J. Dougherty, J. Porphyrins Phthalocyanines 5 (2001) 105.

[10] X. Feng, S. Zhang and X. Lou, Colloid Surface B 107 (2013) 220.

[11] M. Song, R. Zhang, Y. Sai, F. Gao, H. Chi, L. Gang, B. Chen and X. Wang, Biomaterials 27 (2006) 4230.

[12] Q. Li, X. Wang, X. Lu, H. Tian, H. Jiang, G. Lv, D. Guo, C. Wu and B. Chen, Biomaterials 30 (2009) 4708.

[13] R. Cai, Y. Kubota, T. Shuin, H. Sakai, K. Hashimoto and A. Fujishima, Cancer Res. 52 (1992) 2346.

[14] R. Zanella, S. Giorgio, C.R. Henry and C. Louis, J. Phys. Chem. B 106 (2002) 7034.

[15] H. Jung, D. Moon and J. Lee, J. Nano. Mater. 2012 (2012) 1.

[16] Y. He, X.C. Wang, P.K. Jin, B. Zhao and X. Fan, Spectrachim. Acta, Part A 72 (2009) 876.

[17] J. Zhang, S. Rana, R.S. Srivastava and R.D.K. Misra, Acta Biomater. 4 (2008) 40.

[18] F. Muhammad, M. Guo, Y. Guo, W. Qi, F. Qu, F. Sun, H. Zhao and G. Zhu, J. Mater. Chem. 21 (2011) 13406.

[19] P. Wagner, M. Hegner, P. Kernen, F. Zaugg and G. Semenza, Biophys. J. 70 (1996) 2052.

[20] B. Dordi, H. Schonherr and G.J. Vancso, Langmuir 19 (2003) 5780.

[21] L. Sanchez-del-Campo, M.F. Montenegro, J. Cabezas-Herrera and J.N. Rodriguez-Lopez, Pigm. Cell Melanoma R. 22 (2009) 588.

[22] C. Bonechis, A. Donati, R. Lampariello, S. Martini, M.P. Picchi, M. Ricci and C. Rossi, Spectrochim. Acta, Part A 60 (2004) 1411.

[23] C.M. Alexander, K.L. Hamner, M.M. Maye and J.C. Dabrowiak, Bioconjugate Chem. 25 (2014) 1261.

[24] H. Okabayashi, I. Shimizu, E. Nishio and C.J. O'Connor, Colloid Polym. Sci. 275 (1997) 744.

[25] J.B. Rosenholm, P. Stenius and I. Danielsson, J. Colloid Interface Sci. 57 (1976) 551.

[26] C. Sun, R. Sze and M. Zhang, J. Biomed. Mater. Res. 78A (2006) 550.

[27] A. Vora, A. Rega, D. Dollimore and K.S. Alexander, Thermochim. Acta 392 (2002) 209.

[28] M.G.A. El-Wahed, M.S. Refat and S.M. El-Megharbel, Spectrochim. Acta, Part A 70 (2008) 916.

[29] K. Nohara, H. Hidaka, E. Pelizzetti and N. Serpone, J. Photochem. photobiol., A 102 (1997) 265.

[30] Z. Chu, Y. Huang, L. Li, Q. Tao and Q. Li, Biomaterials 33 (2012) 7540.

[31] J.-S. Chang, K.L.B. Chang, D.-F. Hwang and Z.-L. Kong, Environ. Sci. Technol. 41 (2007) 2064.

[32] S. Miotti, P. Facheris, A. Tomassetti, F. Bottero, C. Bottini, F. Ottone, M.I. Colnaghi, M.A. Bunni, D.G. Priest and S. Canevari, Int. J. Cancer 63 (1995) 395.

[33] E. Song, Z. Zhang, Q. Luo, W. Lu, Y. Shi and D. Pang, Clin. Chem. 55 (2009) 955.

[34] J. Xu, Y. Sun, J. Huang, C. Chen, G. Liu, Y. Jiang, Y. Zhao and Z. Jiang, Bioelectrochemistry 71 (2007) 217.

[35] K. Matsui, M. Karasaki, M. Segawa, S.Y. Hwang, T. Tanaka, C. Ogino and A. Kondo, Med. Chem. Commun. 1 (2010) 209.

[36] Z. Li, L. Mi, P.-N. Wang and J.-Y. Chen, Nanoscale Res. Lett. 6 (2011) 356.

[37] X. Feng, H. Guo, K. Patel, H. Zhou and X. Lou, Chem. Eng. J. 244 (2014) 327.

Figure Captions

Fig. 1. A schematic illustration of the synthesis of the FA-conjugated TiO_2-SiO_2 core-shell structure.

Fig. 2. (a) FTIR spectra of FA and NHS-FA; (b) ^1H NMR spectra of NHS-FA.

Fig. 3. (a) FESEM and (b) TEM images of P25, TS, TS-NH_2, and TS-FA.

Fig. 4. FTIR spectra in the range of (a) 100-4000 cm^{-1} and (b) 1300-1700 cm^{-1}.

Fig. 5. (a) TGA curves of P25, TS, TS-NH_2, and TS-FA nanoparticles and (b) Phenol concentration changes with time.

Fig. 6. Cell viability after being treated with P25, TS, and TS-FA for 6 h and 24 h respectively: (a) L929 and (b) KB cells. $^{*}p<0.05$ as compared with control. All data are expressed as mean±SD and n=3. The error bar is based on the standard deviation.

Fig. 7. (a) Hemolysis activity and (b) Photo-killing of KB cells by P25 (□), TS (▨), and TS-FA (▩). $^{*}p<0.05$ as compared with the results obtained at 12.5 μg ml^{-1}. $^{\dagger}p<0.05$ as compared with control. $^{\dagger\dagger}p<0.05$ as compared with P25-treated cells at the same concentration. All data are expressed as mean±SD and n=3. The error bar is based on the standard deviation.

Fig.8. Laser confocal micrographs of KB cells. All images were recorded after 6 h of incubation with 100 μg ml^{-1} nanoparticles at 37 ^{o}C. Upper panel (a): fluorescence images; Lower panel (b): the corresponding differential interference contrast micrographs.

Fig.1

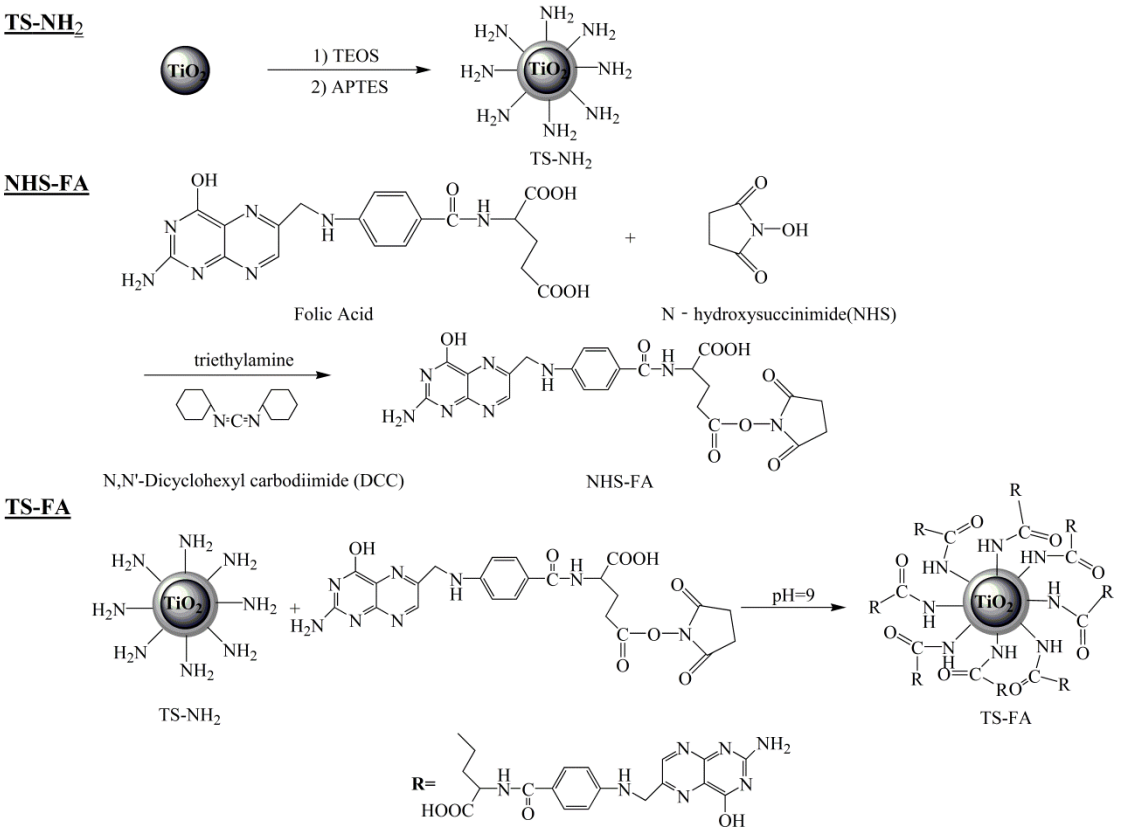
TS-NH2
1) TEOS
2) APTES
TS-NH2
NHS-FA
Folic Acid
N - hydroxysuccinimide(NHS)
triethylamine
N,N'-Dicyclohexyl carbodiimide (DCC)
NHS-FA
TS-FA
pH=9
TS-NH2
TS-FA
R=

Fig. 2

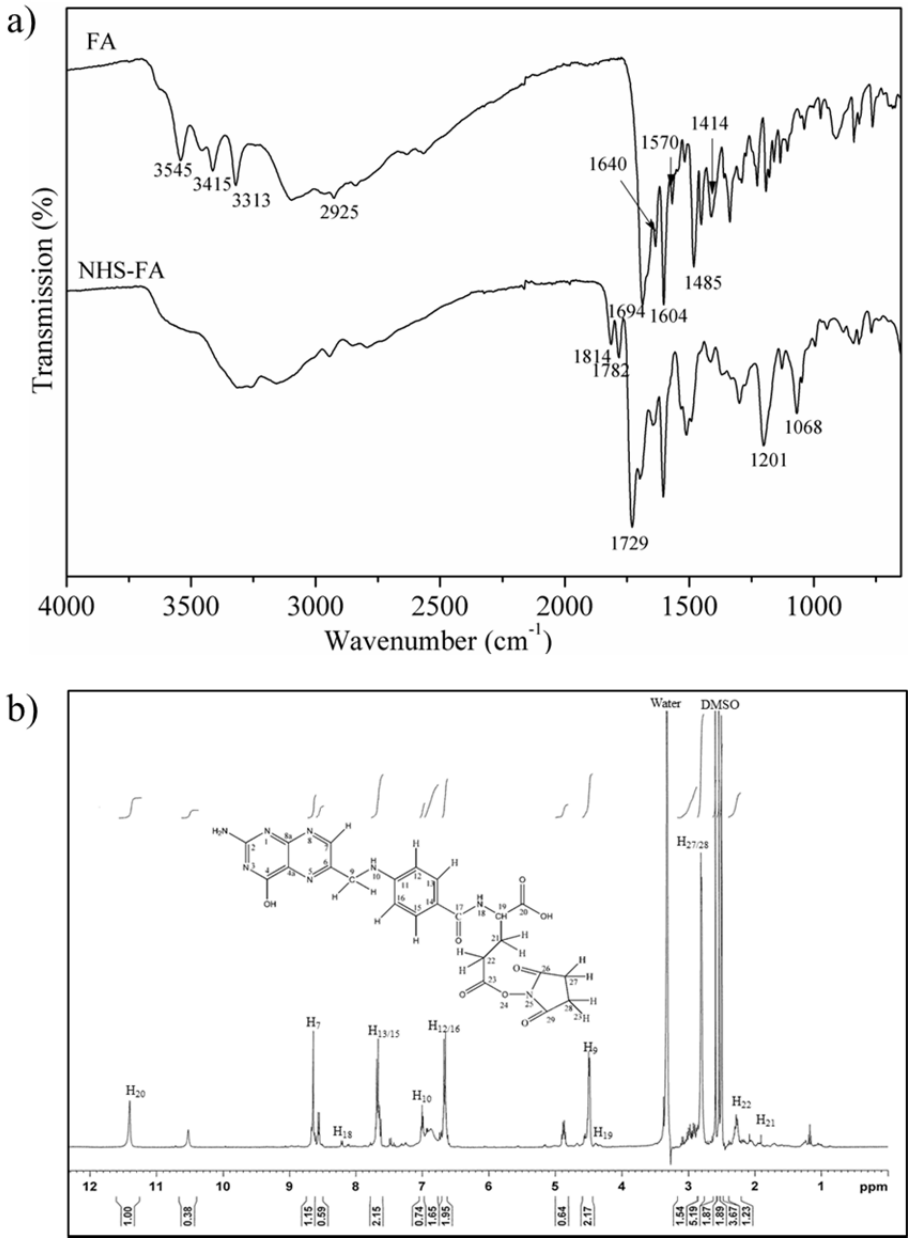
a)
FA
NHS-FA
Transmission (%)
3545
3415
3313
2925
1640
1570
1414
1485
1694
1604
1814
1782
1729
1201
1068
4000
3500
3000
2500
2000
1500
1000
Wavenumber (cm-1)
b)
Water
DMSO
H27/28
H7
H13/15
H12/16
H9
H20
H10
H18
H19
H22
H21
12
11
10
9
8
7
6
5
4
3
2
1
ppm

Fig. 3

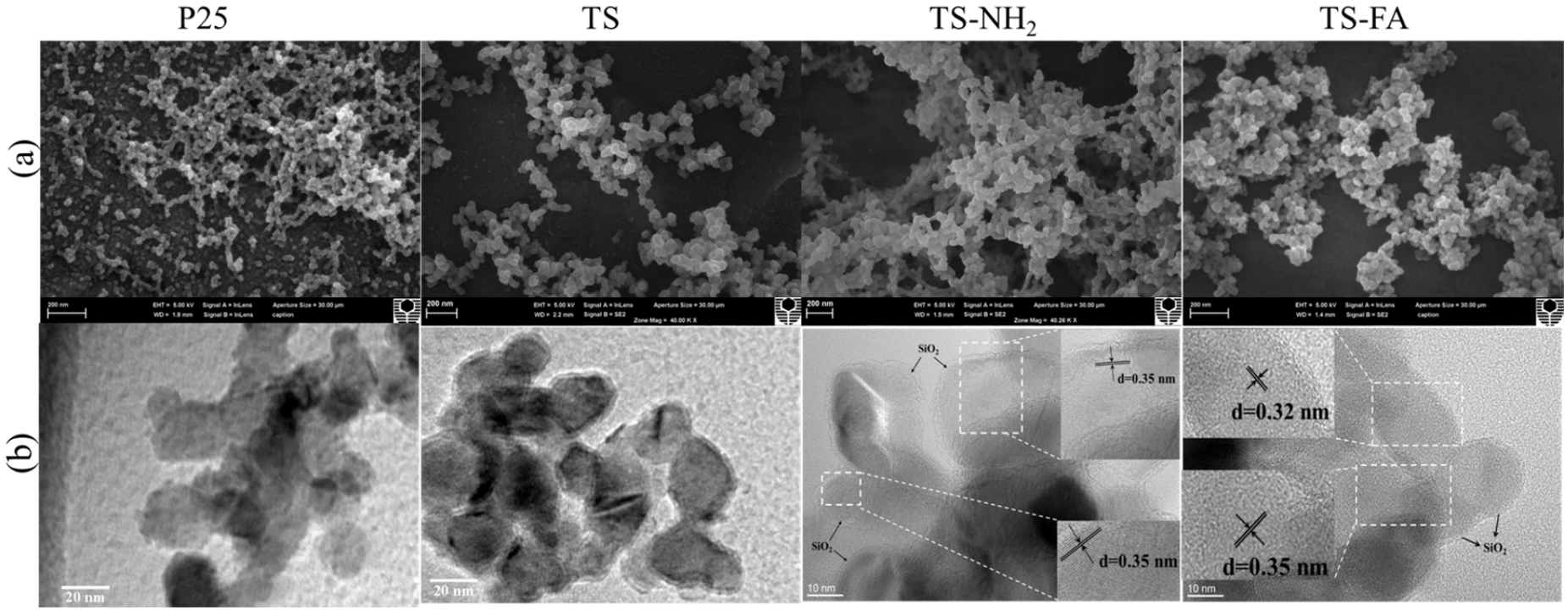
P25
TS
TS-NH2
TS-FA
(a)
(b)
20 nm
20 nm
SiO2
d=0.35 nm
SiO2
d=0.35 nm
10 nm
d=0.32 nm
d=0.35 nm
SiO2
10 nm

Fig. 4

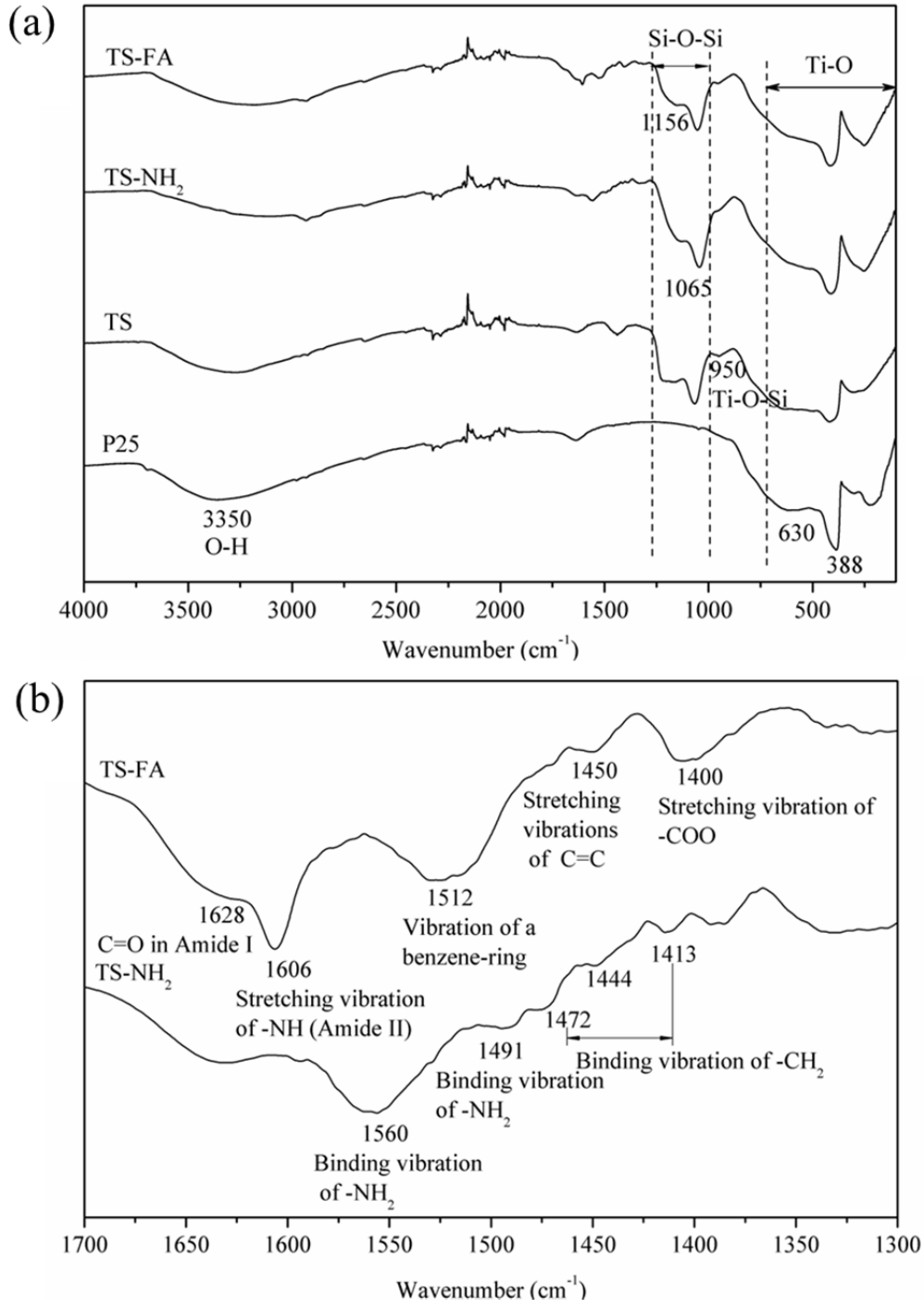
(a)
TS-FA
Si-O-Si
Ti-O
1156
TS-NH2
1065
TS
950
Ti-O-Si
P25
3350
O-H
630
388
4000
3500
3000
2500
2000
1500
1000
500
Wavenumber (cm-1)
(b)
TS-FA
1450
Stretching
vibrations
of C=C
1400
Stretching vibration of
-COO
1628
C=O in Amide I
1512
Vibration of a
benzene-ring
TS-NH2
1606
Stretching vibration
of -NH (Amide II)
1444
1413
1472
1491
Binding vibration
of -NH2
Binding vibration of -CH2
1560
Binding vibration
of -NH2
1700
1650
1600
1550
1500
1450
1400
1350
1300
Wavenumber (cm-1)

Fig.5

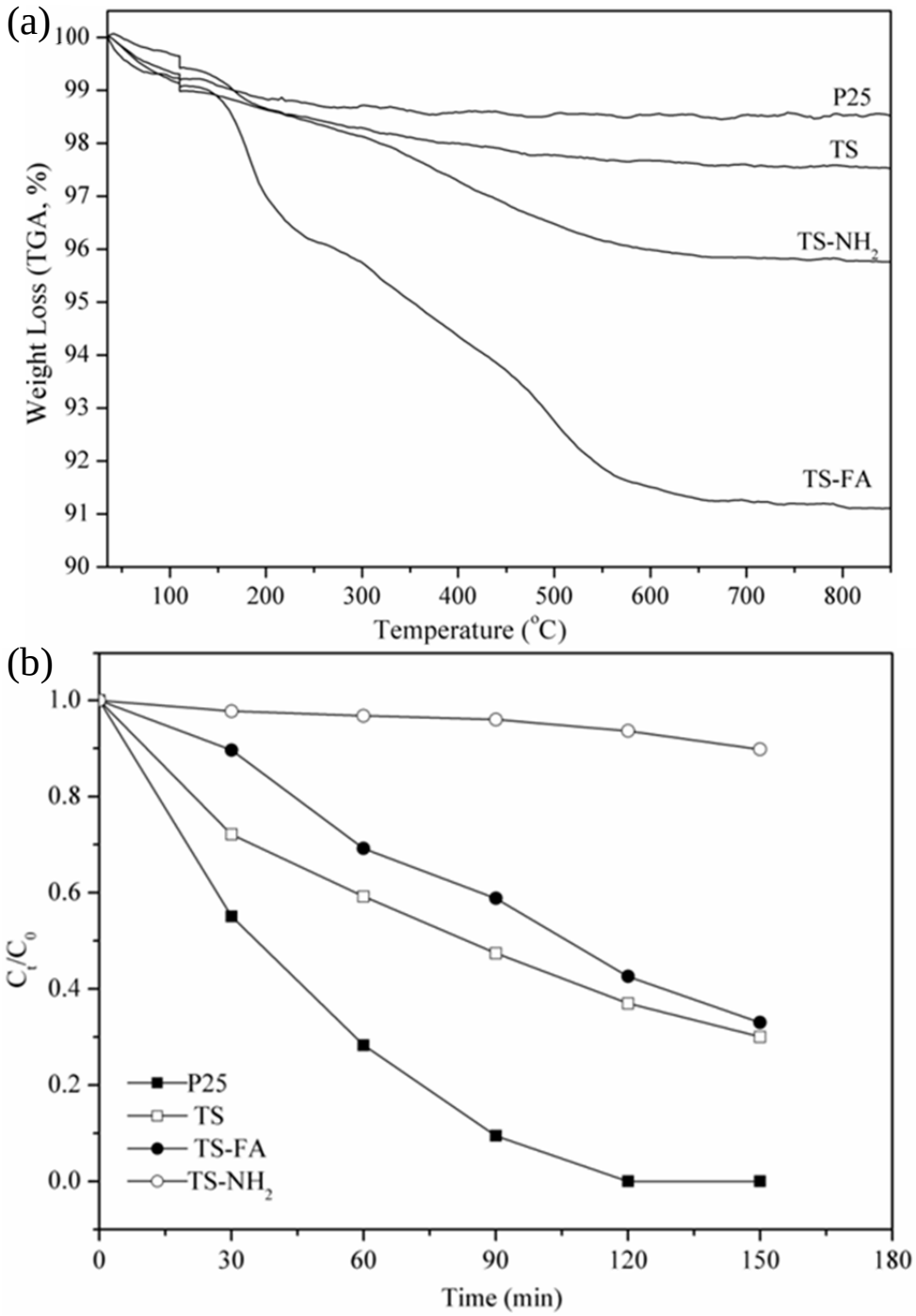
(a)
Weight Loss (TGA, %)
Temperature (°C)
P25
TS
TS-NH2
TS-FA
(b)
C_t/C_0
Time (min)
P25
TS
TS-FA
TS-NH2

Fig. 6

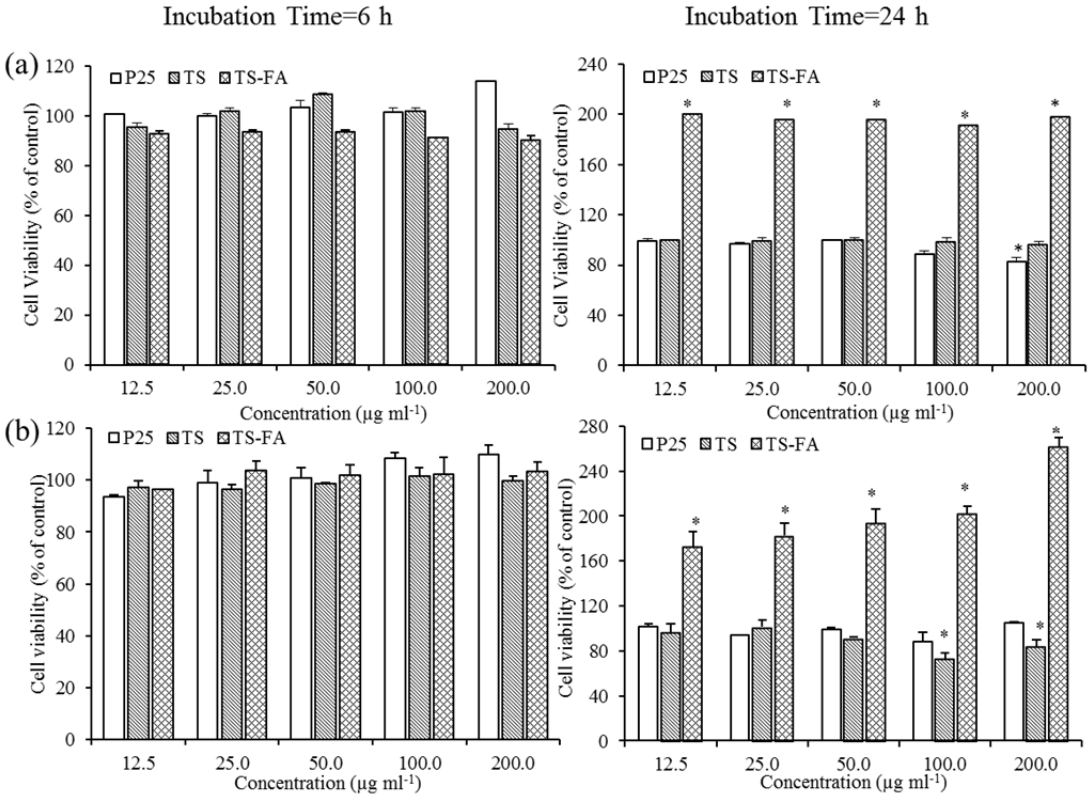
Incubation Time=6 h
Incubation Time=24 h
(a)
(b)
P25
TS
TS-FA
Cell Viability (% of control)
Cell viability (% of control)
Concentration (μg ml-1)
12.5
25.0
50.0
100.0
200.0
*

Fig. 7

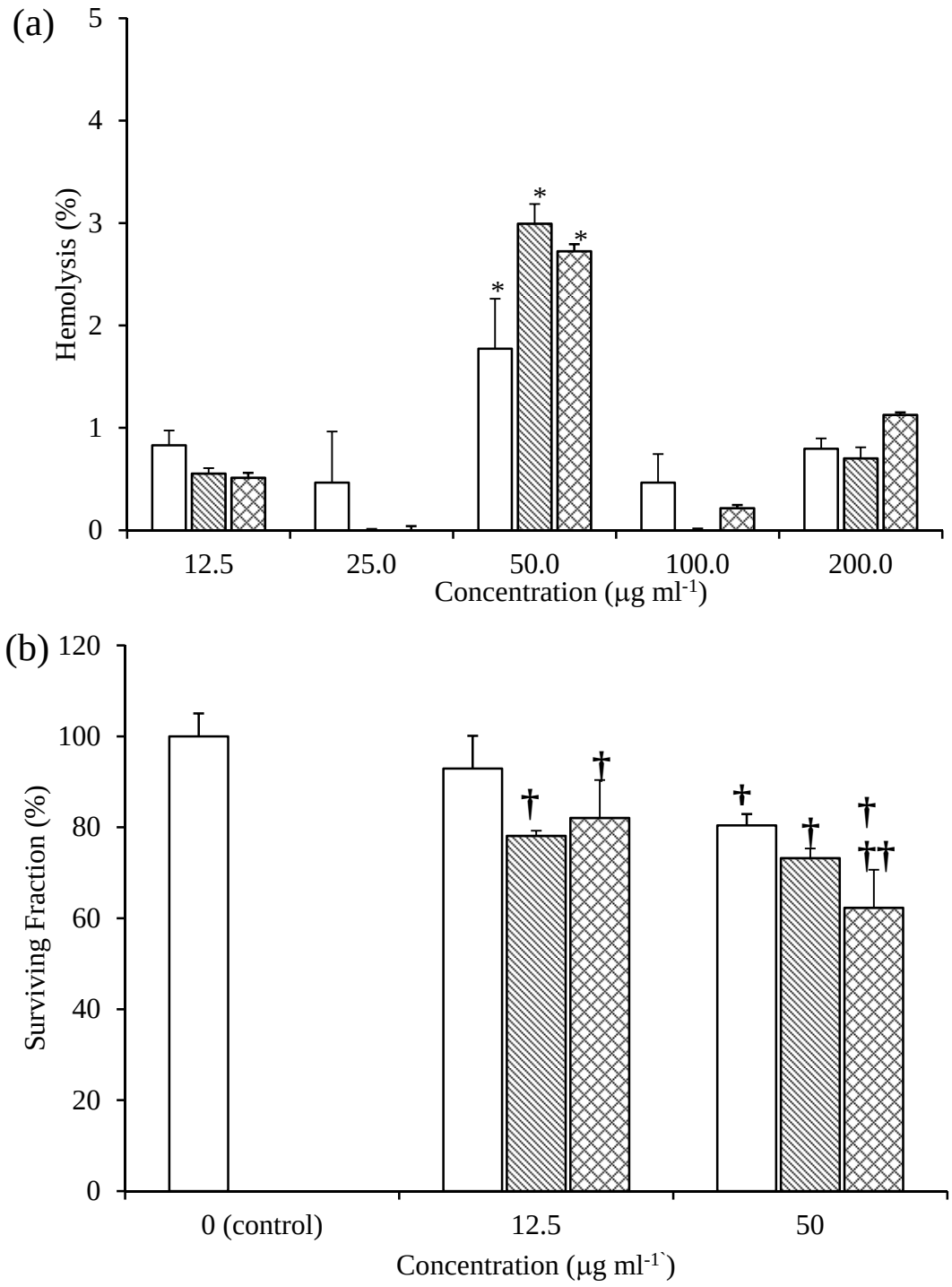
(a)
Hemolysis (%)
0
1
2
3
4
5
*
*
*
12.5
25.0
50.0
100.0
200.0
Concentration (μg ml-1)
(b)
Surviving Fraction (%)
0
20
40
60
80
100
120
†
†
†
†
†
†
0 (control)
12.5
50
Concentration (μg ml-1`)

Fig. 8